Applied Catalysis B: Environmental 327 (2023) 122449

Contents lists available at ScienceDirect

Applied Catalysis B: Environmental

journal homepage: www.elsevier.com/locate/apcatb

Unraveling the role of Fe_5C_2 in CH_4 formation during CO_2 hydrogenation over hydrophobic iron catalysts

Zhenzhou Zhang [a], Baojian Chen [a], Lingyu Jia [a], Wenqi Liu [a], Xinhua Gao [b], Jian Gao [a], Bo Meng [a], Yisheng Tan [d], Yurong He [b,d,*], Weifeng Tu [a,**], Yi-Fan Han [a,c,***]

[a] Engineering Research Center of Advanced Functional Material Manufacturing of Ministry of Education, School of Chemical Engineering, Zhengzhou University, Zhengzhou 450001, China
[b] State Key Laboratory of High-efficiency Utilization of Coal and Green Chemical Engineering, School of Chemistry and Chemical Engineering, Ningxia University, Yinchuan 750021, China
[c] State Key Laboratory of Chemical Engineering, East China University of Science and Technology, Shanghai 200237, China
[d] State Key Laboratory of Coal Conversion, Institute of Coal Chemistry, Chinese Academy of Sciences, Taiyuan 030001, China

ARTICLE INFO

Keywords:
Hydrophobic iron catalyst
H2O partial pressure
Pathways of CH4 formation
Product distribution regulation
Reaction mechanisms

ABSTRACT

The production of value-added hydrocarbons by CO_2 hydrogenation over iron (Fe) catalysts is an emerging platform reaction in CO_2 utilization. However, CH_4 forming in all hydrogenation reactions is undesirable. We focus on the role of Fe_5C_2 active species in CH_4 formation during CO_2 hydrogenation catalysis. Thus, Fe_5C_2 was manipulated by covering a hydrophobic shell to clarify the pathway of CH_4 formation. By a combination of TPSR, in situ spectroscopies and DFT calculations, the variation in the mechanism of CH_4 formation with the content of hydrophobic shell has been revealed. Meanwhile, the enhancement of H_2O retention on the hydrophobic shell surface of Fe_5C_2 was found to inhibit the activation of CO_2 by increasing energy barriers of C-C coupling reactions. Deep insights into the tunable role of Fe_5C_2 in the formation of CH_4 can help for the further design of high performance catalysts for this reaction.

1. Introduction

Iron (Fe) catalysts have attracted wide research interest in the conversion of CO_2 into paraffins [1], olefins [2], aromatics [3], etc., due to their high-performance and ready availability. In particular, these catalysts have excellent potential in the utilization of both CO_2/CO and greener H_2 in the future, which is a long strategy, or "low carbon economics", enforced by all governments worldwide. However, improving the selectivity toward value-added products is a major challenge in the design of such catalytic processes. Among all products, CH_4 as an undesirable byproduct is produced in all those reactions. It is not only decreasing the reaction selectivity but also consuming more hydrogen, which is one precious raw material.

Iron carbides (FeC_x), which are more accurately described as Fe_5C_2 species, have been regarded as active species or sites for CO_2 hydrogenation [4–6]. By modifying the structure of Fe_5C_2 species, many efforts have been made to regulate product distribution. The alkali metal additives Na [7–9], K [10,11] and Rb [12,13] can tune the electronic structure at the interfaces of iron-based catalysts, thus improving the adsorption strength of CO_2 and the formation of the interface between Fe_5C_2 and carbonates, and reducing the olefin desorption energy barrier. The transitional metal oxide additives Mn [7,14], Zn [2,7,15], Cu [16] and Ce [17,18] were used to adjust the content and particle size of Fe_5C_2 and increase the number of oxygen vacancies. Consequently, these bimetallic Fe-M catalysts could reduce the reduction energy barrier of iron species by regulating the electronic characteristics of carbon species. More oxygen vacancies on the surface of m-ZrO_2 and the electron-donating ability of Fe boosted the charge-transfer between Fe and ZrO_2 [19], and the particle size effect of Fe_5C_2 was divided into the effects on the primary and secondary reactions on ZrO_2 surfaces [20].

* Corresponding author at: State Key Laboratory of High-efficiency Utilization of Coal and Green Chemical Engineering, School of Chemistry and Chemical Engineering, Ningxia University, Yinchuan 750021, China.
** Corresponding author.
*** Corresponding author at: Engineering Research Center of Advanced Functional Material Manufacturing of Ministry of Education, School of Chemical Engineering, Zhengzhou University, Zhengzhou 450001, China.
E-mail addresses: hyr@nxu.edu.cn (Y. He), weifengtu@zzu.edu.cn (W. Tu), yifanhan@ecust.edu.cn (Y.-F. Han).

https://doi.org/10.1016/j.apcatb.2023.122449
Received 25 November 2022; Received in revised form 3 January 2023; Accepted 8 February 2023
Available online 13 February 2023

Currently, the tunable role of iron carbides on CH_4 formation during CO_2 hydrogenation is still not clear despite extensive researches on these fundamental issues. A major challenge we face is the strong chain growth ability of iron carbides during CO_2 hydrogenation. CH_4 inevitably exists in the product distribution, but less knowledge about the tunable role of Fe_5C_2 on CH_4 formation is available.

Another overwhelming challenge is how to modify the structure of both iron carbides and iron oxides precisely. The C/H/O chemical potential in the reduction atmospheres (H_2 vs. CO vs. CO/H_2) can regulate the route of Fe_5C_2 formation, which follows the order of Fe_2O_3→Fe_3O_4→Fe in H_2 atmosphere. Subsequently, Fe species are carbonized into Fe_5C_2 in reaction atmosphere (CO_2/H_2) [14,18],while an alternative route of Fe_2O_3→Fe_3O_4→Fe_5C_2 in the CO and CO/H_2 atmosphere has been proposed [21]. The interaction between the support and Fe_5C_2 could alter the carbon-rich surface and lower disorder of carbon species, which is associated with the Fe/C ratio and Fe_5C_2 [22]. Therefore, both the size of the Fe_5C_2 nanoparticles and the Fe_5C_2/Fe_xO_y ratio could change dynamically during the reaction. The effect of the reaction environment variation on the structure of iron carbides could twist the effect of the particle size variation of Fe_5C_2 on CH_4 formation. For example, the low coordination corners and edges on small Fe_5C_2 particles are presumed to promote CH_4 formation [20], whereas the selectivity toward CH_4 is irrelevant to the particle size of Fe_5C_2 on bare iron catalysts [23]. As a consequence, the uncontrollable C/H/O chemical potential of iron carbides can override the function of Fe_5C_2 on CH_4 formation, leading to contradictory conclusions.

CH_4 formation is usually an inevitable reaction during CO_2 hydrogenation [24,25], and CH_4 is considered a prototype C1 byproduct because its formation involves the cleavage of C-O and the formation of C-H. Therefore, a deep understanding of the intricate role of Fe_5C_2 in CH_4 formation would be helpful for elucidating the variation mechanisms of CH_4 formation and the termination of the C-C coupling reaction during CO_2 hydrogenation. For this goal, a controllable intensity [24] of iron carbide catalyst needs to be prepared. CO_2 and H_2O in feedgas have identified to play a key role in the oxidation of iron carbides [26], the effect of H_2O partial presure on oxidation is stronger than that of CO_2 [27]. Therefore, the framework of iron carbides can be precisely reconstructed by controlling the H_2O partial pressure in the oxidic atmosphere. Recently, hydrophobic Fe_5C_2 showed high thermal and chemical stabilities in the conversion of syngas to olefins [28]. This inspired us to develop hydrophobic Fe-based catalysts (designated Fe-Si-C) to control the intensity of iron carbide under real reaction conditions and consequently regulate CH_4 formation on Fe_5C_2.

In this work, Fe_5C_2 was manipulated by covering a series of hydrophobic shell content, the H_2O partial pressure was regulated, and the strong chain growth ability of Fe_5C_2 was suppressed to some extent, causing to the ratio of CH_4/C_{2+} to increase to 3.7, which is presently the highest CH_4/C_{2+} ratio over Fe_5C_2 during CO_2 hydrogenation. In particular, the pathways of CH_4 formation on Fe_5C_2 were clarified by elaborately designing in situ spectroscopy, TPSR experiments and DFT calculations. The study of the tunable role of Fe_5C_2 in the formation of CH_4 reported here will not only elucidate the tunable mechanism of CH_4 formation pathways in CO_2 hydrogenation but also help to design other functional catalysts for lowering the inevitable byproducts of CH_4.

2. ExperimentaL section

2.1. Catalyst preparation

2.1.1. Preparation of Fe_2O_3

Fe_2O_3 was prepared by a coprecipitation method, and 12.33 g of $FeCl_2{\cdot}4\ H_2O$ was dissolved into 200 mL of ultrapure water (> 18.2 MΩ). Subsequently, 620 mL of sodium carbonate solution (1.2 M) was added dropwise to the ferrous chloride solution at a speed of 0.04 $cm^3{\cdot}s^{-1}$ at 20 ± 3 °C. During the addition process, a magnetic stirrer was kept running. Then the precipitate stood for 2 h at 25 °C. The precipitate was then centrifuged and washed with ultrapure water to remove Na and other impurities, the detailed procedures was reported in previous literature [52]. The precursor was dried in an oven at 60 °C for 12 h and then removed for grinding. After grinding, the sample was put into a muffle furnace, heated from room temperature to 400 °C with a ramping rate of 8 °C/min, and then kept at a constant temperature for 4 h. Finally, it was reduced to room temperature.

2.1.2. Preparation of Fe_2O_3 @SiO_2

Fe_2O_3 @SiO_2 was prepared by Stober's method [28]. The precursor Fe_2O_3 powder was dispersed into an ethanol solution under ultrasonic to obtain a uniform suspension. The solution concentration was 0.0104 mol/L. Tetraethyl silicate (TEOS) was added and stirred at 500 rpm for 4 h. Then ammonia (25–28%, AR) and ultra-pure water were added and stirred for another 4 h, and TEOS:$NH_3{\cdot}H_2O$:H_2O= 1:5:20. The resulting mixture was washed with ethanol 3–5 times and dried in 100 °C air for 12 h, and then Fe_2O_3 @SiO_2 was obtained.

2.1.3. Preparation of Fe_2O_3 @SiO_2-C

The prepared Fe@SiO_2 precursor was preheated in a 120 °C oven for 12 h, cooled to room temperature and added to n-ethane [N-hexane (AR)]. Then, trimethylchlorosilane (TMCS) was added, and the mixture was ultrasonically pretreated at room temperature for 3 h, washed with n-ethane 3–5 times, and then dried in an oven at 80 °C for 12 h to obtain the desired sample named Fe_2O_3 @SiO_2-C_x (X = 0.25, 0.50), where X represents Fe@SiO_2/g added to x mL TMCS.

2.2. Catalytic reaction

The hydrogenation of the CO_2 reaction was carried out in a fixed-bed reactor. The catalysts (0.1 g) were diluted with SiO_2 (1:1). Before the reaction, the catalysts were initially reduced by 20% CO for 10 h, and the reduction conditions were 0.5 MPa, 350 °C and 50 mL/min. Then, the catalysts were subjected to a flow of H_2/CO_2/Ar, the reaction conditions of 1.5 MPa, 320 °C, 10,000 mL/(g·h) and H_2/CO_2/Ar= 3:1:3 were implemented unless otherwise specified.

All products were detected by an online gas chromatograph (GC), and the carbon balance ranged from 90% to 100%. The conversion of CO_2 was calculated by a TCD using a TDX-01 column. CO and CO_2 were hydrogenated to CH_4 by a methane converter, and then CO, CO_2 and CH_4 were detected by FID 1 using a Porapak-Q column. Hydrocarbons were analyzed by FID 2 using an HP-PLOT-Q column. The calculation method of CO_2 conversion, CO selectivity, product selectivity and content of H_2O in the outlet are according to the following equations (Eqs. 1–4).

$$CO_2\ \text{Conversion} = \frac{M(CO_2\text{inlet}) - M(CO_2\text{outlet})}{M(CO_2\text{inlet})} \times 100\% \quad (1)$$

$$\text{CO Selectivity} = \frac{M(COoutlet)}{M(COoutlet) + \sum nM(CnHmoutlet)} \times 100\% \quad (2)$$

$$\text{Hydrocarbon selectivity} = \frac{nM(CnHmoutlet)}{M(COoutlet) + \sum nM(CnHmoutlet)} \times 100\% \quad (3)$$

$$M_{H_2O\ \text{outlet}} = 2(M_{CO_2\text{inlet}} - M_{CO_2\text{outlet}}) - M_{CO\ \text{outlet}} \quad (4)$$

In these equations, M(CO_2 inlet) and M(CO_2 outlet) represent the number of moles of CO_2 at the inlet and outlet, M(CO outlet) and $M_{H2Ooutlet}$ indicate the number of moles of CO and H_2O at the outlet of reactor, and M(C_nH_m outlet) denotes the number of moles of C_nH_m at the outlet of the reactor.

2.3. Catalyst characterization

XRD patterns were recorded on a Bruker D8 Advance X-ray powder

diffractometer. The X-ray source was CuKα with a tube voltage of 40 kV, a tube current of 40 mA and a scanning step of 0.02°.

Water-droplet contact angle tests were performed on a Biolin Theta Flex. The transmission electron microscopy (TEM) results were obtained on Talos 200 A (FEI, America) electron microscopes with an acceleration voltage of 200 kV.

Room temperature ^{57}Fe Mössbauer spectra of the catalysts were measured on a Topologic 500 A spectrometer equipped with ^{57}Co(Rh) as the γ-ray radioactive source moving in constant acceleration mode. All of the spectra were fitted by using the MössWinn4.0pre program to determine parameters such as the isomer shift (IS) and quadrupole splitting (QS). The IS values and Doppler velocities were calibrated using an α-iron foil.

FTIR spectroscopy was conducted in a refection mode in a reaction chamber (Harrick Scientific) equipped with ZnSe windows mounted onto a Thermo Scientific iS50 Fourier transform infrared spectrometer equipped with a smart MCT detector cooled by liquid nitrogen. The infrared spectra in the range between 4000 cm^{-1} and 400 cm^{-1} were measured by averaging 32 scans with a resolution of 4 cm^{-1}.

In situ IR spectra of intermediate species were recorded as follows: The fresh precursors of the catalysts were first purged under Ar flow at 50 °C and 0.1 MPa for 30 min to be a background, the temperature was increased to 350 °C and 0.1 MPa, and finally, the system was switched to 5% CO/Ar for 2 h. After the reduction process, the temperature was decreased to 320 °C and 0.1 MPa, and the system was switched to H_2/CO_2/Ar (3:1:3) for 1 h. Subsequently, the temperature was decreased to 50 ℃ and 0.1 MPa, and the IR spectra were recorded. The in situ IR spectra of the hydrogenation of intermediate species were recorded as follows: The spent catalyst was chosen and purged under Ar flow at 50 °C and 0.1 MPa for 30 min to be the background, and then the temperature was increased to 320 °C and 0.1 MPa and held for 30 min. After that, a flow of 5% H_2/Ar was introduced to treat the catalysts for 5 min and 30 min, respectively. Finally, the temperature was decreased to 50 °C and 0.1 MPa, and the IR spectra were recorded.

Ar-TPD and CO_2-TPD were carried out by the following procedure: 50 mg of the catalyst sample powder was loaded into a quartz tube (inner diameter: 4.5 mm) in a microplug flow reactor with the bottom supported by quartz cotton. The sample was heated to 300 °C for 0.5 h at a ramping rate of 10 °C/min in 30 mL /min of an Ar flow, and then cooled to 50 °C. (1) For Ar-TPD, the sample was heated to 800 °C at a ramping rate of 5 °C/min. (2) For CO_2-TPD, CO_2 was absorbed for 1 h at 50 °C; the Ar was then switched, and the sample was heated to 800 °C at a ramping rate of 5 °C/min. The exhaust gas was detected by a Hidden CATLAB connected to a gas analytical mass spectrometry QIC20.

H_2-TPR was carried out by the following procedure: 50 mg of the catalyst sample powder was loaded into a quartz tube (inner diameter: 4.5 mm) in a microplug flow reactor with the bottom supported by quartz cotton. The sample was heated to 300 °C for 1.0 h at a ramping rate of 10 °C/min in 30 mL /min of an Ar flow, and then cooled to 80 °C. The flow of H_2 and Ar mixture (the volume ratio of H_2/Ar was 5/95) in 30 mL /min was then switched, and the sample was heated to 600 °C at a ramping rate of 5 °C/min. The exhaust gas was detected by a Hidden CATLAB connected to a gas analytical mass spectrometry QIC20.

2.4. DFT methods and models of Fe_5C_2 compounds

2.4.1. Methods

All spin-polarized density functional theory (DFT) calculations were performed using the Vienna Ab initio Simulation Package (VASP) [29,30]. Electron-ion interactions were described by projector augmented wave potentials (PAW) [31,32]. Exchange-correlation effects were described by the Perdew-Burke-Ernzerhof (PBE) functional [33] and generalized gradient approximation (GGA) [34]. The plane wave cutoff energy was specified to be 400 eV, and electron smearing via a 2nd-order Methfessel-Paxton [35] technique with a width of 0.2 eV was employed to ensure energy with errors less than 1 meV per atom. The convergence criteria for electronic self-consistent interactions and forces were set to 10^{-4} eV and 0.03 eV/Å, respectively. Brillouin zone sampling was performed using the Monkhorst-Pack scheme [36]. To study the reactions, transition states (TSs) were estimated by the climbing image nudged elastic band (CI-NEB) method [37,38], and vibrational frequencies were analyzed to evaluate a transition state with only one imaginary frequency along with the reaction coordinate.

2.4.2. Models

Fe_5C_2(510) surface is demonstrated to be one of the major exposed surfaces according to Wulff construction [39–41], and the effects of H_2O molecules on the carbide surfaces are represented by the Fe_5C_2(510) facet. To study the hydrogenation properties of CO_2 on the iron-based catalyst, the detailed mechanisms of the reactions were studied on the Fe_5C_2(510) surface (Fig. S9). We used $p(2\times2)$ supercells containing five carbon and three iron atom layers with a thickness of 5.18 Å for the surface slab model. The slab has a size of 9.96 Å × 12.64 Å, in which the top three atom layers with adsorbates are relaxed and the bottom five atom layers are fixed in their bulk position. According to the lattice sizes, 2 × 2 × 1 k-point grid sampling within the Brillouin zones was set. The vacuum gap space was set as 15 Å to avoid significant interactions between the two slabs.

3. Results and Discussion

3.1. Structural characterization and catalytic performance

The particle size of fresh Fe_2O_3 was measured to be 20–25 nm and it was transferred to a mixture of Fe_3O_4 and iron carbides, and the size of the Fe_3O_4 is 30–35 nm for the spent catalysts (Figs. S1a, 1b and Table S1). It is likely that the particle size of the iron species was mildly affected by the hydrophobic shell. The increase in the content of the Si-O-C hydrophobic shell on the surface of the iron catalysts completely changed the H_2O droplet contant angle from approximately 20° to 146° (Figs. 1a and 1c). The hydrophobic shell stagnated during the reaction and was still covered uniformly on the spent catalysts (Figs. 1d, 1e, S1b, S1c, S5 and S6). The catalysis of CO_2 hydrogenation (Figs. 2a, 2b, 2c, 2d, S2, S3 and S4) shows that the selectivity toward CH_4 increased obviously from 37.4% to 76.2%, while that toward C_2 + decreased from 50.3% to 20.5% and CH_4 was a predomiant product. Fe_5C_2 is a well-known active species for carbon chain growth.[7] The ^{57}Fe-Mössbauer spectra (Fig. 2e and Table S3) showed a decrease in the content of Fe_5C_2 from 59.0% to 32.0%, which is consistent with the decline in selectivity to the C_2 + products. The minimum content of Fe_5C_2 exihibited the highest selectivity to CH_4 and the lowerest selectivity to CO and C_{2+}, leading to the ratio of CH_4/CO increasing from 2.6 to 23.1 and that of CH_4/C_{2+} increasing from 0.6 to 3.7. A question may arise regarding the effect of the hydrophobic shell on the mass-transfer resistance of reactants and products, whereas several previous studies [28,42] on the conversion of syngas to C_{2+} hydrocarbons have revealed that the same function of hydrophobic shell can be ignored completely. Besides, textural properties of the iron-based catalysts in Table S2 confirms that the decrease of pore volume and pore diameter due to the hydrophobic shell can also be ignored.

In the hydrogenation of CO_2 over iron catalysts, the role of Fe_5C_2 in CH_4 formation during CO_2 hydrogenation is usually neglected due to the strong carbon chain growth ability over Fe_5C_2. The comparative data listed in Table S4 show that Fe-Si-$C_{0.50}$ in this work has the highest ratio of CH_4/C_{2+} and CH_4/CO, which indicates that the hydrophobic shell prohibits the formation of CO and C_{2+} during CO_2 hydrogenation. With an increase in the ratio of CH_4/C_{2+} and CH_4/CO, CH_4 can be regarded as the main product but C_2 + and CO as byproducts, therefore, the tunable mechanisms of Fe_5C_2 on CH_4 formation pathways must be investigated further.

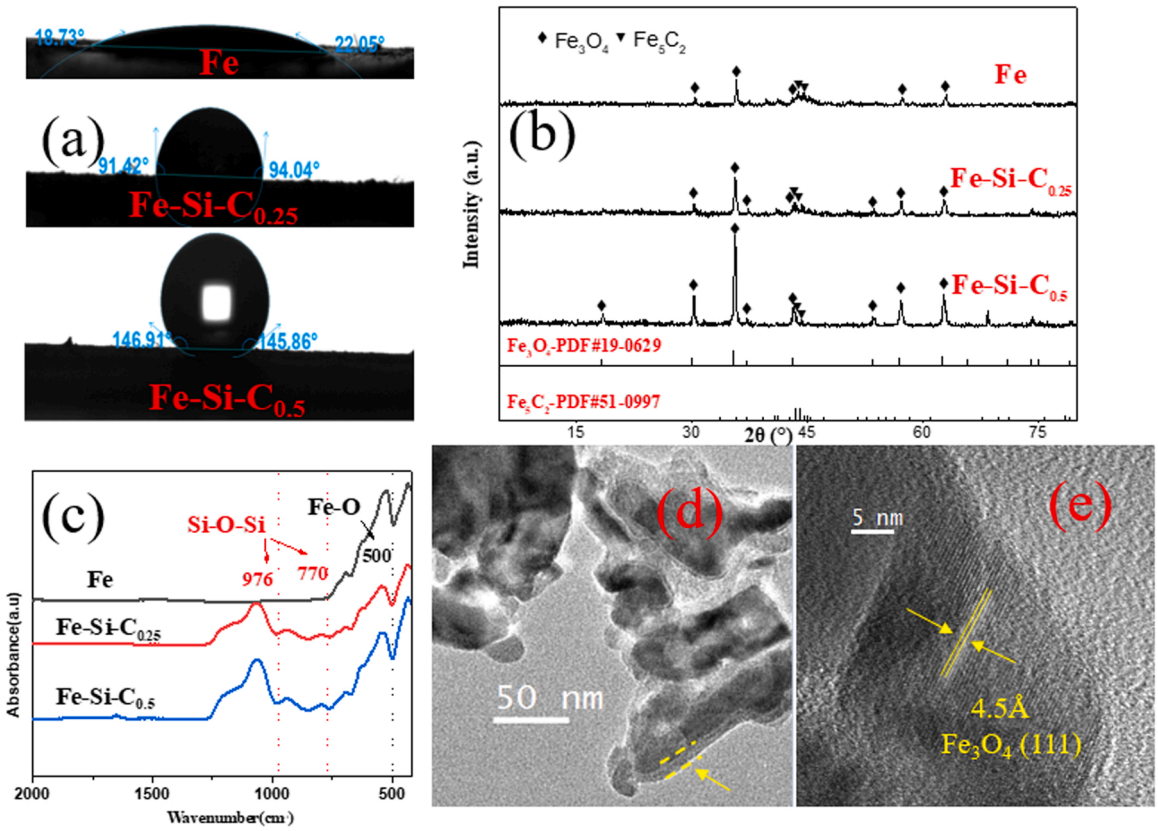

Fig. 1. Structural characterization of Fe, Fe-Si-$C_{0.25}$ and Fe-Si-$C_{0.5}$. **(a)** Water-droplet contact angle tests. (**b**) The XRD patterns of spent Fe-based catalysts. **(c)** FTIR spectra of the fresh catalysts. **(e** and **f)** TEM images of the spent Fe-Si-$C_{0.5}$.

3.2. Water distribution analysis

$$CO_2 + H_2 = CO + H_2O, \eta RWGS = \frac{PCOPH2O}{PCO2PH2}\frac{1}{KRWGS} \quad (5)$$

$$CO_2 + 4H_2 = CH_4 + H_2O, \eta methanation = \frac{PCH4P2H2O}{PCO2P4H2}\frac{1}{K methanation} \quad (6)$$

The approach-to-equilibrium values (η_{RWGS} and $\eta_{methanation}$) in Eq.5-6 show the extent to which the RWGS and CO_2 methanation reaction is shifted from chemical equilibrium during CO_2 hydrogenation. P_i is the partial pressure of species i (i = CO, H_2O, CO_2, CH_4 or H_2), and K_{RWGS} and $K_{methanation}$ denote the chemical equilibrium constants for both RWGS and CO_2 methanation reactions, respectively. $\eta_{methanation}$ remained at ~0, while η_{RWGS} decreased from 0.670 to 0.013 with increasing the hydrophobic shell content (Fig. 3a). The value of $K_{methanation}$ ($1.06*10^5$) was much larger than that of K_{RWGS} (0.0327) when the reaction temperature was 320 °C, which accounts for the small variation in $\eta_{methanation}$. Compared to the variation in $\eta_{methanation}$, the variation in η_{RWGS} was probably derived from the increase in the content of the hydrophobic shell. The H_2O content in the outflow resulting from unit CO_2 conversion remained unchanged (Fig. 3a), which indicates that the hydrophobic shell can only affect the distribution of H_2O. Several studies [28,42,43] on syngas conversion have demonstrated that the hydrophobic shell can promote the desorption of H_2O and decrease the partial pressure of H_2O. However, the amount of H_2O formed during CO_2 hydrogenation was twice as much as the amount formed during CO hydrogenation, and the transformation of H_2O from Fe_5C_2 to hydrophobic shell was inhibited to some extent, increasing the H_2O pressure on the surface of Fe_5C_2 (Fig. 3b). An increase in the amount of Fe_3O_4 in spent catalysts (Table S3) suggests that Fe_5C_2 covered with the hydrophobic shell was oxidized with the increase in H_2O pressure, which also confirms that the H_2O pressure on the surface of Fe_5C_2 increased to some extent. Therefore, the hydrophobic shell regulated the water distribution and increased the H_2O partial pressure on the surface of Fe_5C_2.

3.3. DFT calculations of CO_2 hydrogenation on the Fe_5C_2(510) surface

Given that with the hydrophobic shell on the catalysts, H_2O molecules are confined only within the surface of iron carbides, the impacts of H_2O on CO_2 hydrogenation should be considered. By means of DFT calculations, the modulation of H_2O molecules on the reaction mechanisms (Fig. S10), including CO_2 activation, CH_4 formation and carbon chain growth, has been proposed over a typical stable Fe_5C_2(510) surface [41,44]. As illustrated in Fig. 4a, on the surface of pure Fe_5C_2(510), CO_2 undergoes facial C-O cleavage with a tiny barrier of 0.30 eV instead of hydrogenation steps to form COOH and HCOO species. This result is similar to that on the Fe and Fe–Cu bimetallic surfaces [16], although HCOO is an intermediate for CO_2 activation on other catalysts [45]. After the removal of O by H_2O formation and desorption (**P-B**, CO*+O*+2H* → **P-C**, CO*+2H*), direct C-O dissociation occurs with a lower barrier than CO activation through an HCO intermediate, which is inconsistent with previous studies [41,46]. With H_2O formation and H_2 adsorption (**P-D**, C*+O*+2H* → **P-E**, C*+ 2H*), surface carbon (C*) could be created. All the corresponding structures of the surface intermediates and transition states are given in Fig. 5, while the facial H_2 dissociation and diffusion steps are ignored.

On the H_2O-doped surface (Fig. 4b), CO_2 activation also takes place through the direct C-O cleavage path (**W-A**, CO_2*+2H*+H_2O*→ **W-D**, C*+O*+2H*+$2H_2O$*), and the corresponding structures of the surface intermediates and transition states are given in Fig. 6. However, the E_a for this route is higher than that on the pure Fe_5C_2(510) surface,

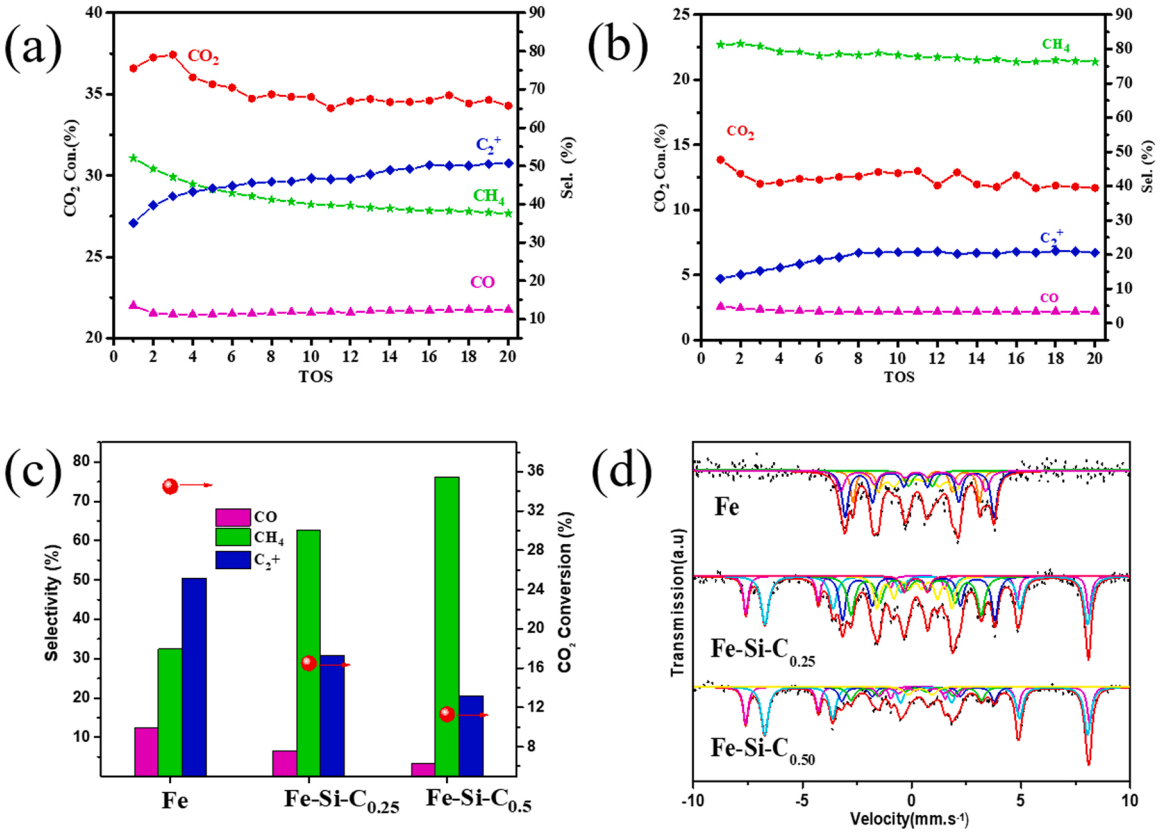

Fig. 2. **(a** and **b)** Catalytic performance of CO_2 hydrogenation over Fe and Fe-Si-$C_{0.5}$ with TOS. **(c)** Product distribution of Fe, Fe-Si-$C_{0.25}$ and Fe-Si-$C_{0.5}$. **(d)** ^{57}Fe-Mössbauer spectra of the spent catalysts.

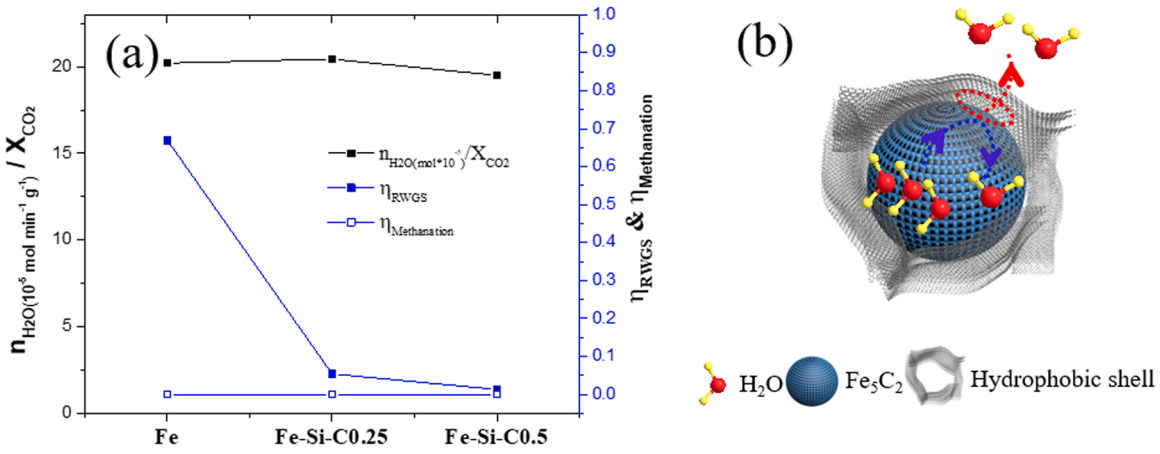

Fig. 3. **(a)** The approach to equilibrium factor for the RWGS step (Eq.5), the methanation step (Eq.6) and the H_2O content in the out flow resulted from unit CO_2 conversion. **(b)** Schematic diagram of the effect of the hydrophobic shell on H_2O distribution.

especially for CO dissociation (2.05 eV vs. 1.11 eV). It is noted that H_2O molecules formed during O hydrogenation are retained on the surface, since previous experimental results revealed that the hydrophobic shell could increase the H_2O partial pressure. The high barrier for CO activation is due to steric effects as well as electron transfer from the surface to H_2O molecules because more net electrons of the surface Fe atoms are beneficial for CO activation via back donation [47,48]. In general, CO_2 activation is suppressed by surface H_2O adsorption, which leads to a decrease in CO_2 conversion, as we observed in the experiments.

In addition to CO_2 activation, both CH_4 formation and C-C coupling were also investigated (Figs. 7 and 8). For CH_4 formation, following CO_2 activation, the reactions went through similar potential energy paths on both the pure and the H_2O doped surfaces. Even with three H_2O molecules adsorbed on the surface, the effective energy barriers are very close (1.04 eV vs. 1.09 eV). The hydrogenation of CH_3 is the rate-determining step, as proposed previously [49,50]. For the chain growth reaction, the coupling of HC-CH and C-CH is easier than that of CH_x-CH_y ($0 \leq x \leq 3$, $0 \leq y \leq 3$) on the Fe_5C_2(510) surface [40]. According to our calculations, the activation energy for HC-CH is even lower than C-CH coupling (Fig. 9). Therefore, HC-CH coupling is taken as the probe reaction for carbon chain growth. The activation energy of 0.98 eV was estimated on the pure surface and was elevated to 1.21 eV with two H_2O molecules adsorbed near the active site. Since CH_4 formation and C-C coupling are competing reactions, the selectivity toward methane was increased by

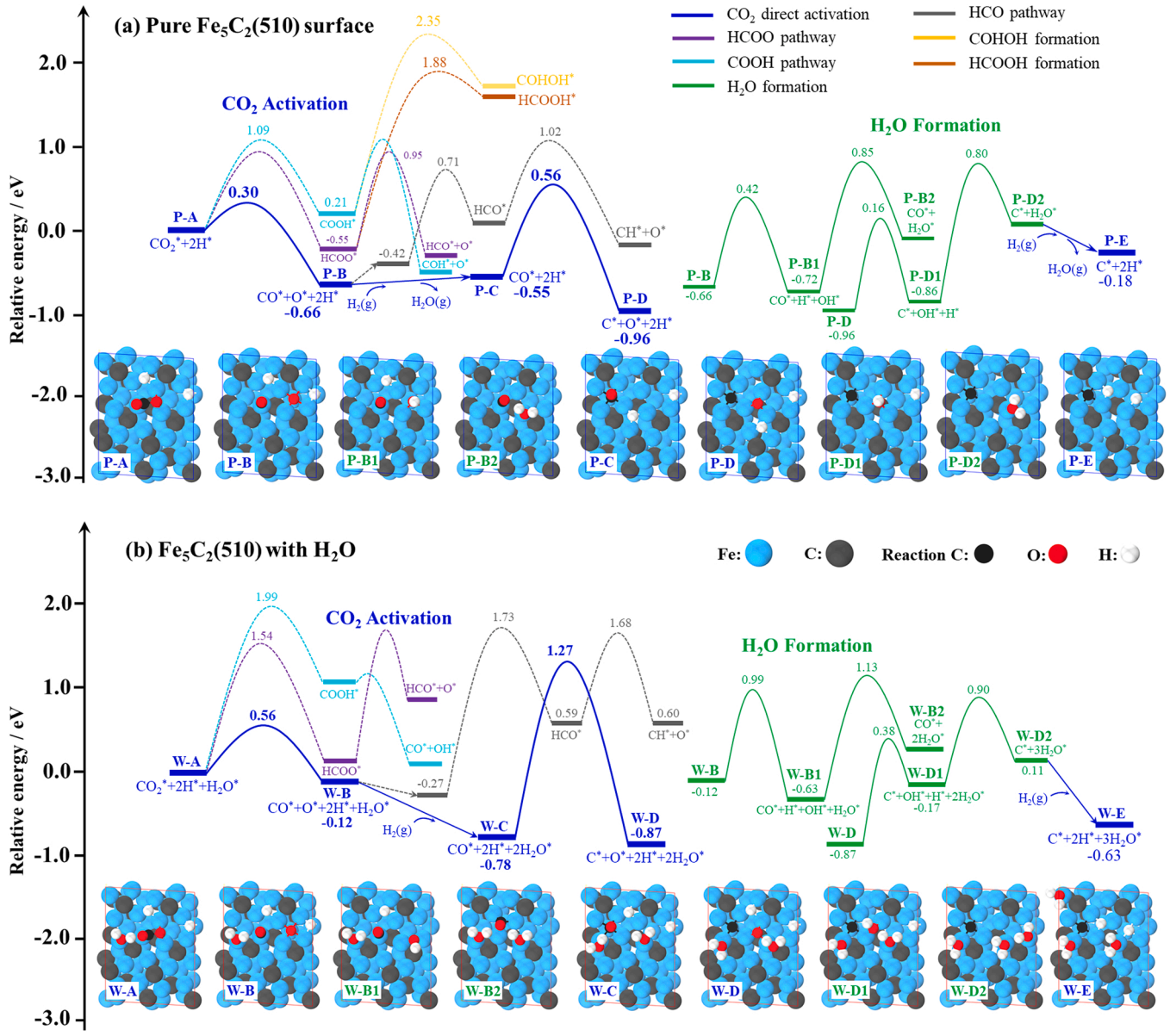

Fig. 4. The detailed energy profiles and the intermediate structures of CO_2 hydrogenation on the (**a**) pure and (**b**) H_2O doped Fe_5C_2(510) surfaces. The relative energy is given with respect to the initial state.

the suppression of chain growth. In addition, the C-C coupling reaction requires spatially continuous active sites, and an increase in surface H_2O molecules may block the active sites and thus hinder long-chain hydrocarbon production.

Above all, surface H_2O retention notably affects the electronic and reaction properties of the catalyst. The elevated energy barriers of CO_2 activation as well as the C-C coupling reactions obtained by theoretical calculations account for the suppressed activity and increased ratio of CH_4/C_{2+}. In order to alleviate the situation that an increase in the H_2O retention on the surface of Fe_5C_2 could suppress the activation of CO_2, two suggestions for the catalyst design are proposed. One way is to increase net electrons of the surface Fe atoms for CO activation via back donation by adding electronic donors, consequently the activation energy of CO on the surface of Fe_5C_2 could be decreased. Besides, precisely constructing the catalyst to decrease the H_2O retention on the surface of Fe_5C_2 could promote the conversion of CO_2 to C_2 + products.

3.4. In situ IR exploration of the formation and conversion of intermediate species

The IR spectra in Fig. 10a was obtained under similar reaction conditions as described in Fig. 2. The characteristics of formate species (1580, 1045 cm^{-1}) [51] and CH_x species (2962, 2920, 2854 cm^{-1}) [52] increased with the content of hydrophobic shell, whereas that of carbonate species (1508, 1312 cm^{-1}) [53] underwent an an opposite change. There were still several intermediate species on the surface of the spent catalysts (Fig. 2). The hydrogenation of these intermediate species was also investigated (Fig. 11b). When the spent catalysts were treated with H_2 for 5 min, the bicarbonate species (1628, 1440, 1242 cm^{-1}) [54], carbonate species (1480, 1352 cm^{-1}) [51] and formate species (1585,1376,1352 cm^{-1}) [55] could be more easily eliminated on the surface of Fe-Si-$C_{0.50}$ than the intermediate species on the surface of Fe, whereas CH_x species (2962, 2920, 2854 cm^{-1}) [52] were stable on the surface of Fe and Fe-Si-$C_{0.50}$.

DFT calculations showed that both the formation and hydrogenation of CH_x species are key steps to control CH_4 formation. The intensity of

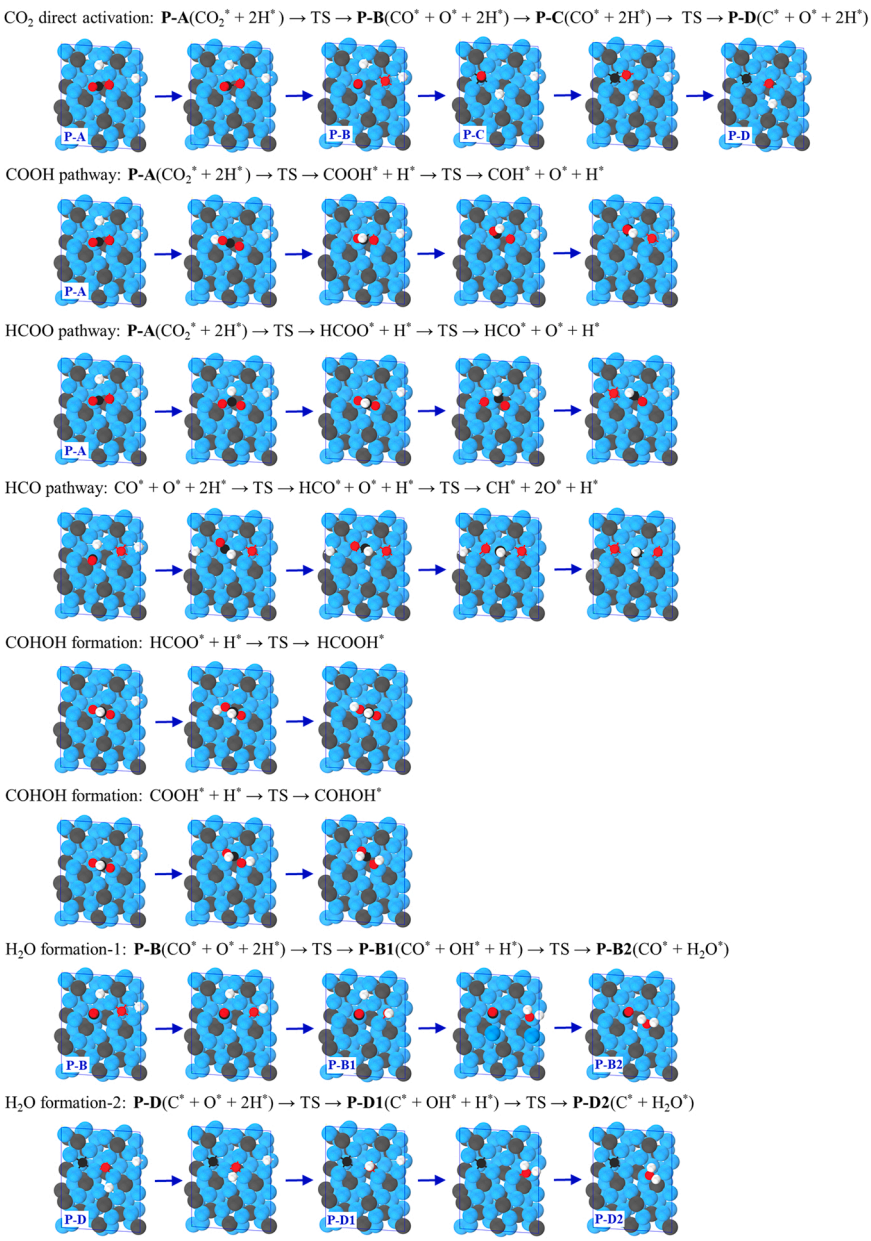

Fig. 5. The structures of the surface intermediates and transition states of CO_2 activation on the pure Fe_5C_2(510) surface.

CH_x species (Fig. 11a) increased with increasing hydrophobic shell content, whereas the intensity of CH_x species (Fig. 11b) remained unchanged when the intermediate species was hydrogenated. Therefore, the increase in H_2O partial pressure can enhance the formation of CH_x species and CH_4, leading to the regulation of CH_4 formation pathways.

In addition, formate species are usually assumed to be the precursor of CH_4 during the reaction [20]. In view of the formation of intermediate species and subsequent hydrogenation, the hydrophobic shell also promotes the production of formate species and further conversion (Figs. 10a and 10b). Therefore, the presence of a hydrophobic shell can regulate the formation and conversion of surface groups containing carbon and oxygen, consequently affecting the formation of CH_4, CO and C_{2+} at a certain level.

3.5. TPSR experiments

The desorption ability of adsorbed CH_4 is another parameter affecting CH_4 formation. The Ar-TPD and CO_2-TPD of the spent catalysts are shown in Figs. 11a and 11b, respectively. The signals of CH_4 were not detected at/below 350 °C, whereas they appeared as the temperature increased to the range of 400–600 °C, which is probably result of the strong chemically bonded CH_4 on the catalyst surface. Table S5 shows that increasing the content of the hydrophobic shell decreased the amount of strongly chemically bonded CH_4 from 2.23 to 0.29. When the spent catalysts were first treated by the flow of CO_2, Table S6 shows that the amount of strongly chemically bonded CH_4 also exhibits a decreasing trend, similar to the results in Ar-TPD.

The hydrogenation reaction of CO_2 occurred at 320 °C, while the CH_4 signals were not detected in the profiles of Ar-TPD and CO_2-TPD below 350 °C; therefore, the weakly absorbed CH_4 is apt to desorb from the surface of spent catalysts; consequently, the weakly absorbed CH_4 did not affect CH_4 formation. With an increase in the content of the hydrophobic shell, the amounts of the strongly chemically bonded CH_4 decreased both in Ar-TPD and CO_2-TPD. The desorbed temperature of strongly chemically bonded CH_4 is approximately 480–550 °C, which is much higher than the reaction temperature of 320 °C and consequently

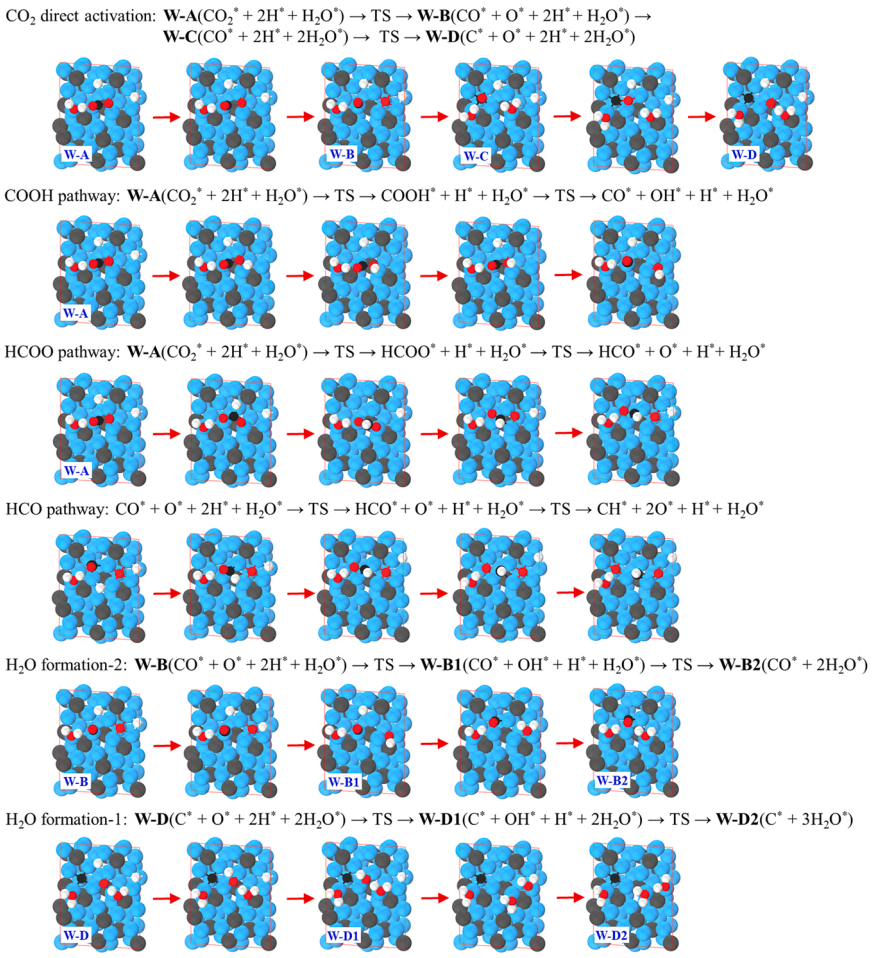

Fig. 6. The structures of the surface intermediates and transition states of CO_2 activation on the H_2O-doped Fe_5C_2(510) surface.

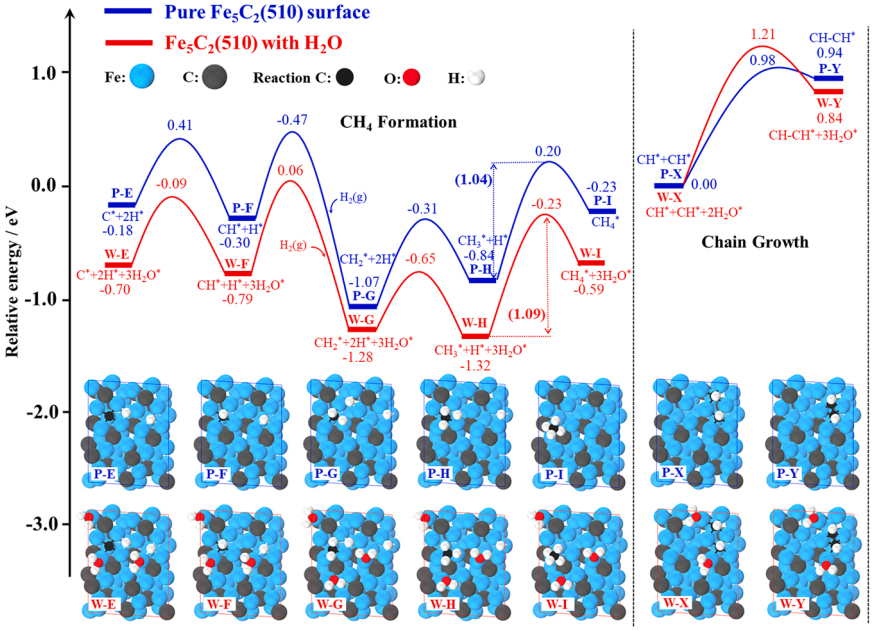

Fig. 7. The energy profiles and the intermediate structures of CH_4 formation and CH-CH coupling on the pure and H_2O doped Fe_5C_2(510) surfaces. The relative energy is given with respect to the initial state of CO_2 activation, and initial states of CH-CH coupling, respectively.

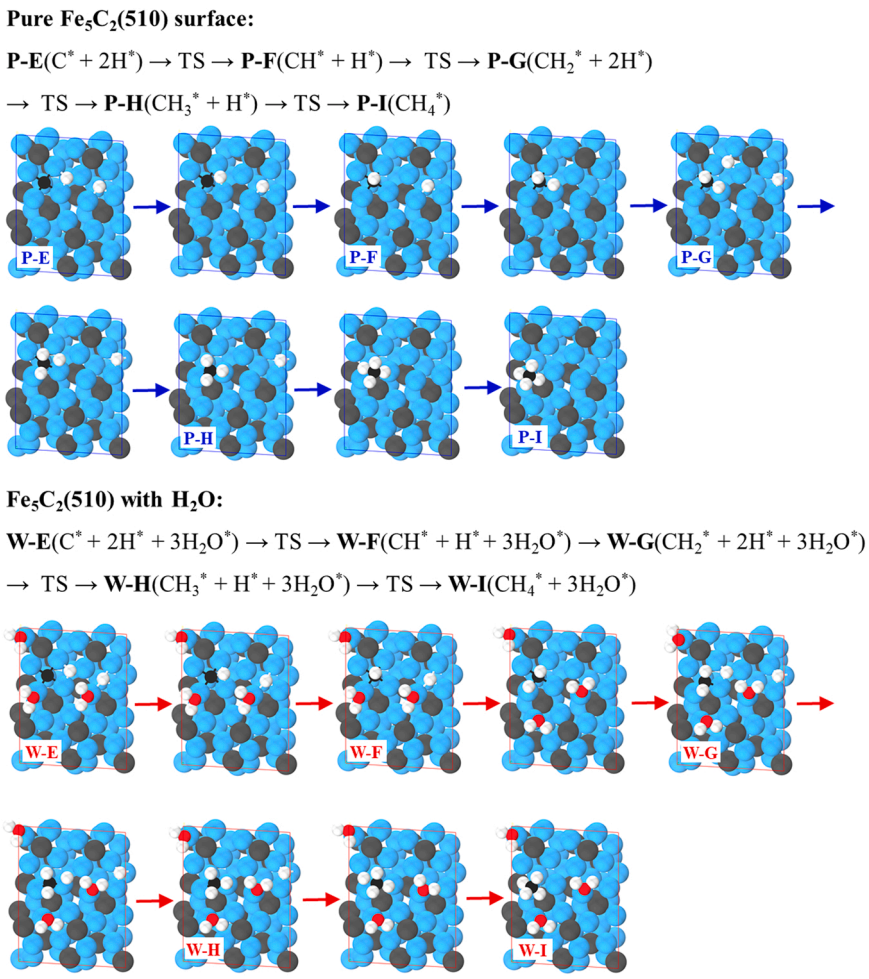

Fig. 8. The structures of the surface intermediates and transition states of CH_4 formation on the pure and H_2O doped Fe_5C_2(510) surfaces.

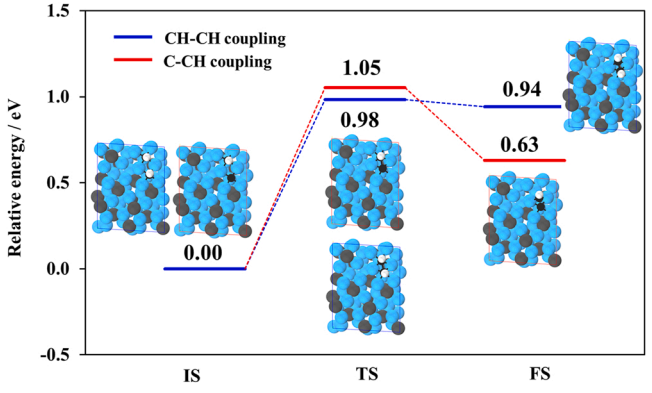

Fig. 9. The detailed energy profiles and corresponding structures of chain growth through C-CH and HC-CH coupling, respectively.

could inhibit the desorption of CH_4. Therefore, the strongly chemically bonded CH_4 could weaken CH_4 formation to some extent.

3.6. The mechanism of CH_4 formation in the presence of a hydrophobic shell

In some cases, the CH_4 and C_{2+} products are separately discussed considering the primary product and the second hydrogenation production in FTS [20,52,56]. However, the activation of CO_2 over Fe_5C_2 has rarely been discussed in both the primary and second reactions. Several previous studies have confirmed the formation of CH_4 via the hydrogenation of carbonate and formate species by IR spectra [24,57], and their conclusions could shed light on their catalyst design, whereas the mechanism of CO_2 activation over Fe_5C_2 is still unclear, and the key factor to answer this challenge is detailed insight into the pathways of intermediate species formation and conversion. In this work, the direct CO_2 activation and the activation of CO_2 with hydrogen are both discussed over Fe_5C_2. The DFT calculations in Figs. 4–6 confirm that direct CO_2 activation through C-O cleavage has a tiny barrier, which is much lower than the steps of hydrogenation to COOH and HCOO species. Therefore, the direct CO_2 activation is proposed, and further CO hydrogenation over Fe_5C_2 is discussed.

In the hydrogenation of CO_2 over iron catalysts, the role of Fe_5C_2 in CH_4 formation during CO_2 hydrogenation is usually neglected due to the strong carbon chain growth ability over Fe_5C_2. In Scheme 1, a plausible mechanism of the hydrophobic shell on CH_4 formation over Fe_5C_2 is proposed. With the presence of a hydrophobic shell, the water distribution in Fig. 3 and the amount of iron oxides in Table S2 confirm that the partial H_2O pressure is increased to some extent (Scheme 1a). The DFT calculations in Figs. 7–8 further confirm that the E_a for the coupling reaction of CH increased from 0.98 eV to 1.21 eV over H_2O-doped Fe_5C_2(510), whereas the E_a values were very close even with three H_2O molecules adsorbed on the surface (1.04 eV vs. 1.09 eV). Therefore, CH_4 formation through the hydrogenation of CH_x was promoted by inhibiting the coupling reaction of CH (Schemes 1b and 1c). Finally, the TPSR experiments in Fig. 11 confirm that the amount of the strongly chemically bonded CH_4 decreases with increasing hydrophobic shell content; consequently, the desorption process of adsorbed CH_4 is promoted

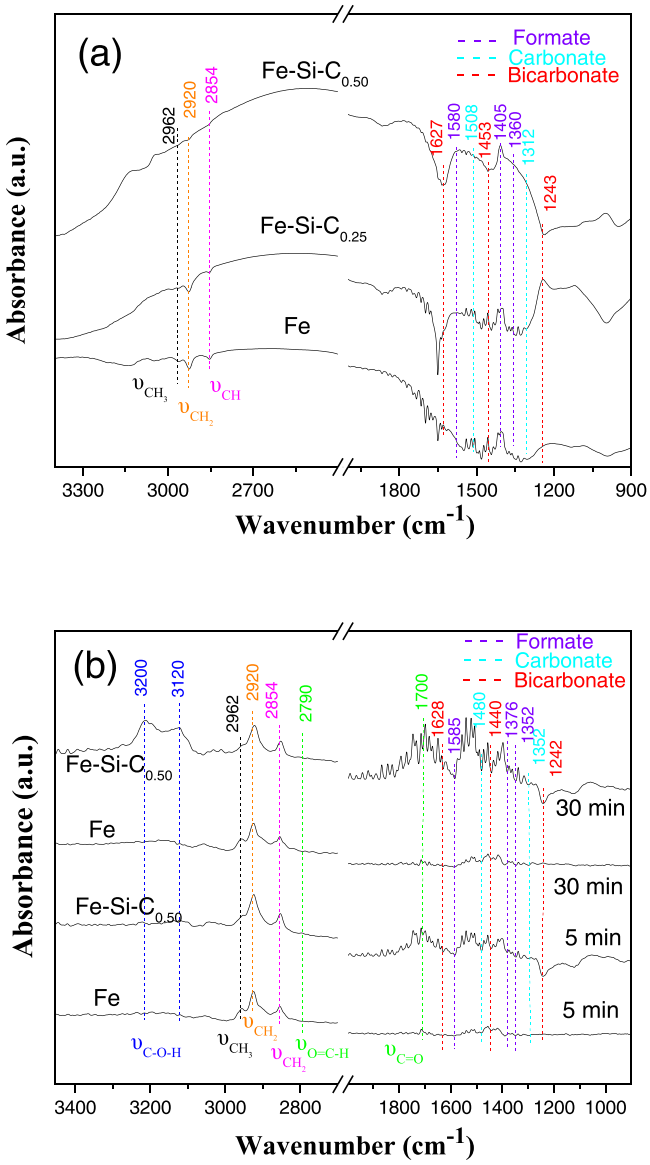

Fig. 10. In situ IR spectra recorded after different reaction conditions. (**a**) The fresh catalysts were purged under an Ar flow at 50 °C for 30 min as a background, and then the temperature was increased to 350 °C and switched to 5% CO/Ar for 2 h. After the reduction process, the temperature was decreased to 320 °C, and the system was switched to H_2/CO_2/Ar (3:1:3) for 1 h. Finally, the temperature was decreased to 50 °C, and the IR spectra were recorded. (**b**) The spent catalyst in Fig. 1e was chosen and purged under Ar flow at 50 °C for 30 min to be a background, and then the temperature was increased to 320 °C and maintained for 30 min. After that, 5% H_2/Ar was introduced to treat the catalysts for 5 min and 30 min, respectively. Finally, the temperature was decreased to 50 °C, and the IR spectra were recorded.

(Scheme 1f). According to the mechanism of CH_4 formation in the presence of a hydrophobic shell, a strategy to decrease the selectivity to CH_4 is proposed·H_2O is inevitable to form on the surface of the Fe_5C_2 during CO_2 hydrogenation, therefore the suggestion for the catalyst design to decrease the selectivity to CH_4 is to accelerate the desorption of H_2O.

In summary, in this work we studied the mechanism of CH_4 formation over Fe_2C_5 with and without a hydrophobic shell coating during CO_2 hydrogenation. CO_2 methanation is a popular reaction in platform reactions in the utilization of CO_2, remarkably reducing the selectivity to value-added products. In combination with in situ spectroscopy, TPSR and DFT calculations, we rationalize the plausible pathways from CO_2

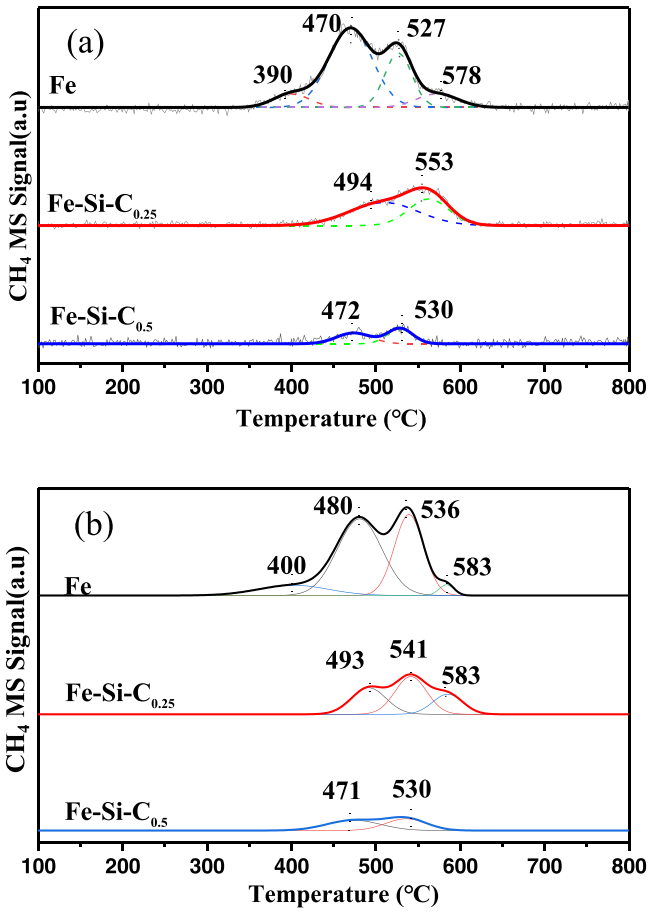

Fig. 11. (**a**) Temperature programmed treatment (Ar-TPD) of the spent catalysts in Fig. 1 under Ar flow. (**b**) CO_2-TPD of the spent catalysts in Fig. 2.

activation, C-O cleavage, and C-H formation steps during the generation of CH_4. The competition mechanisms for the formation of CH_4 and C_2 product were also discussed. We believe that the methodology we have developed for the study of such a complex catalytic system will have high value for the further design of heterogeneous catalysts for CO_2 utilization.

4. Conclusions

In summary, a controllable intensity of iron carbide was manipulated via the surface hydrophobic modification with terminating the carbon chain growth. As a result, the highest CH_4/C_{2+} ratio on the surface of Fe_5C_2 was achieved successfully. An increase in the content of the hydrophobic shell leads to an increase in the H_2O partial pressure on the surface of Fe_5C_2, thus reducing CO_2 conversion by boosting the activation energy of CO_2 hydrogenation. DFT calculations further confirm that the adsorbed H_2O on the surface of Fe_5C_2 elevated the energy barriers of C-C coupling reactions, which makes CH_4 formation easier than its competitive reaction of C-C coupling. According to the mechanism of CH_4 formation in the presence of a hydrophobic shell, a strategy to decrease the selectivity to CH_4 has been proposed·H_2O is inevitable to form on the surface of the Fe_5C_2 during CO_2 hydrogenation, therefore the suggestion for the catalyst design to decrease the selectivity to CH_4 is to accelerate the desorption of H_2O. This innovative way to modify the solid surface inspires us to design high-performance catalysts for CO_2 utilization by suppressing the generation of CH_4.

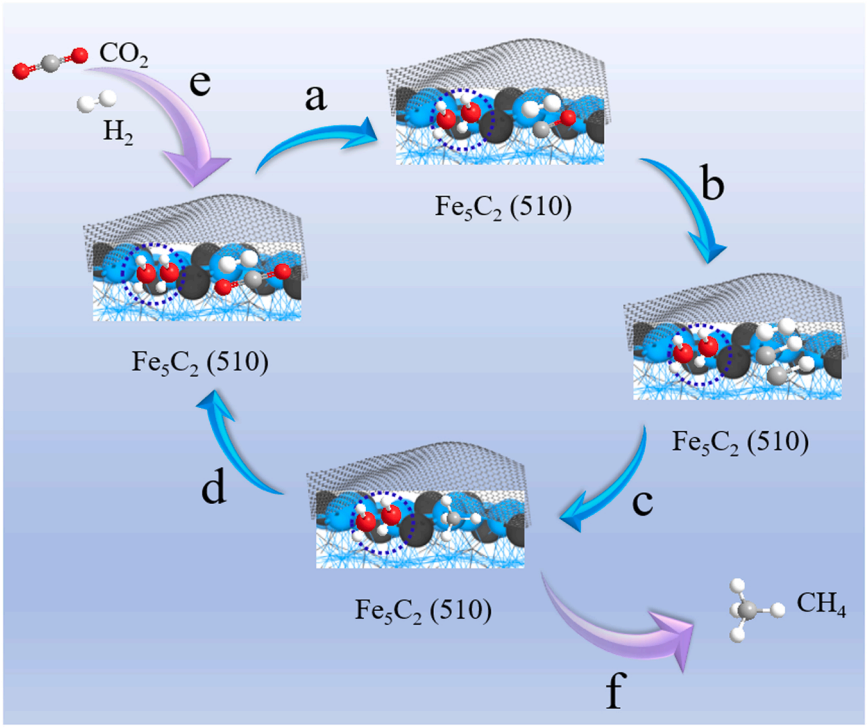

Scheme 1. Plausible mechanism of hydrophobic shell on CH_4 formation over Fe_5C_2.

CRediT authorship contribution statement

Zhenzhou Zhang: Conceptualization, Methodology, Writing, Funding acquisition. **Baojian Chen:** Investigation, Validation, Synthesis, Data curation, Characterization. **Lingyu Jia:** Characterization. **Wenqi Liu:** Data curation. **Xinhua Gao:** Validation. **Jian Gao:** Characterization. **Bo Meng:** Characterization. **Yisheng Tan:** Validation. **Yurong He:** DFT calculation, Funding acquisition, Methodology. Weifeng Tu: Supervision, Funding acquisition, Writing – review & editing. **Yi-Fan Han:** Project administration, Supervision, Funding acquisition, Writing – review & editing.

Declaration of Competing Interest

The authors declare that they have no known competing financial interests or personal relationships that could have appeared to influence the work reported in this paper.

Data Availability

Data will be made available on request.

Acknowledgments

The authors are grateful to the National Natural Science Foundation of China (22208314, 22278379, 22238003, 22078307 and 22002008), Natural Science Foundation of Henan Province (202300410432). The work is also supported by the State Key Laboratory of Coal Conversion (J21-22-902), and State Key Laboratory of High-efficiency Utilization of Coal and Green Chemical Engineering (2022-K05 and 2022-K21). We acknowledge the Center for Advanced Mössbauer Spectroscopy, Dalian Institute of Chemical Physics, CAS, for providing the Mössbauer measurement and analysis.

Appendix A. Supporting information

Supplementary data associated with this article can be found in the online version at doi:10.1016/j.apcatb.2023.122449.

References

[1] J. Wei, Q. Ge, R. Yao, Z. Wen, C. Fang, L. Guo, H. Xu, J. Sun, Directly converting CO_2 into a gasoline fuel, Nat. Commun. 8 (2017) 15174.
[2] C. Zhang, M.J. Xu, Z.X. Yang, M.H. Zhu, J. Gao, Y.F. Han, Uncovering the electronic effects of zinc on the structure of Fe_5C_2-ZnO catalysts for CO_2 hydrogenation to linear α-olefins, Appl. Catal. B-Environ. 295 (2021), 120287.
[3] X. Cui, P. Gao, S.G. Li, C.G. Yang, Z.Y. Liu, H. Wang, L.S. Zhong, Y.H. Sun, Selective production of aromatics directly from carbon dioxide hydrogenation, ACS Catal. 9 (2019) 3866–3876.
[4] B. Liu, S.S. Geng, J. Zheng, X.L. Jia, F. Jiang, X.H. Liu, Unravelling the new roles of Na and Mn promoter in CO_2 hydrogenation over Fe_3O_4-based catalysts for enhanced selectivity to light -olefins, ChemCatChem 10 (2018) 4718–4732.
[5] B. Liang, T. Sun, J. Ma, H. Duan, L. Li, X. Yang, Y. Zhang, X. Su, Y. Huang, T. Zhang, Mn decorated Na/Fe catalysts for CO_2 hydrogenation to light olefins, Catal. Sci. Technol. 9 (2019) 456–464.
[6] J. Wei, R. Yao, Q. Ge, Z. Wen, X. Ji, C. Fang, J. Zhang, H. Xu, J. Sun, Catalytic hydrogenation of CO_2 to isoparaffins over Fe-based multifunctional catalysts, ACS Catal. 8 (2018) 9958–9967.
[7] Y. Xu, P. Zhai, Y. Deng, J. Xie, X. Liu, S. Wang, D. Ma, Highly selective olefin production from CO_2 hydrogenation on iron catalysts: a subtle synergy between manganese and sodium additives, Angew. Chem. Int. Ed. 59 (2020) 21736–21744.
[8] B. Liang, H. Duan, T. Sun, J. Ma, X. Liu, J. Xu, X. Su, Y. Huang, T. Zhang, Effect of Na promoter on Fe-based catalyst for CO_2 hydrogenation to alkenes, ACS Sustain. Chem. Eng. 7 (2019) 925–932.
[9] C.Y. Wei, W.F. Tu, L.Y. Jia, Y.Y. Liu, H.L. Lian, P. Wang, Z.Z. Zhang, The evolutions of carbon and iron species modified by Na and their tuning effect on the hydrogenation of CO_2 to olefins, Appl. Surf. Sci. 525 (2020), 146622.
[10] Y. Han, C.Y. Fang, X.W. Ji, J. Wei, Q.J. Ge, J. Sun, Interfacing with carbonaceous potassium promoters boosts catalytic CO_2 hydrogenation of iron, ACS Catal. 10 (2020) 12098–12108.
[11] C.G. Visconti, M. Martinelli, L. Falbo, A. Infantes-Molina, L. Lietti, P. Forzatti, G. Iaquaniello, E. Palo, B. Picutti, F. Brignoli, CO_2 hydrogenation to lower olefins on a high surface area K-promoted bulk Fe-catalyst, Appl. Catal. B-Environ. 200 (2017) 530–542.
[12] M.K. Gnanamani, H.H. Hamdeh, W.D. Shafer, S.D. Hopps, B.H. Davis, Hydrogenation of carbon dioxide over iron carbide prepared from alkali metal promoted iron oxalate, Appl. Catal. A-Gen. 564 (2018) 243–249.
[13] J.J. Wang, Z.Y. You, Q.H. Zhang, W.P. Deng, Y. Wang, Synthesis of lower olefins by hydrogenation of carbon dioxide over supported iron catalysts, Catal. Today 215 (2013) 186–193.

[14] Z.Z. Zhang, C.Y. Wei, L.Y. Jia, Y.Y. Liu, C. Sun, P. Wang, W.F. Tu, Insights into the regulation of FeNa catalysts modified by Mn promoter and their tuning effect on the hydrogenation of CO_2 to light olefins, J. Catal. 390 (2020) 12–22.
[15] C. Zhang, C.X. Cao, Y.L. Zhang, X.L. Liu, J. Xu, M.H. Zhu, W.F. Tu, Y.F. Han, Unraveling the role of zinc on bimetallic Fe_5C_2-ZnO catalysts for highly selective carbon dioxide hydrogenation to high carbon alpha-olefins, ACS Catal. 11 (2021) 2121–2133.
[16] X.W. Nie, H.Z. Wang, M.J. Janik, Y.G. Chen, X.W. Guo, C.S. Song, Mechanistic insight into C-C coupling over Fe-Cu bimetallic catalysts in CO_2 hydrogenation, J. Phys. Chem. C 121 (2017) 13164–13174.
[17] F.J. Perez-Alonso, M.L. Granados, M. Ojeda, T. Herranz, S. Rojas, P. Terreros, J.L. G. Fierro, M. Gracia, J.R. Gancedo, Relevance in the Fischer-Tropsch synthesis of the formation of Fe-O-Ce interactions on iron-cerium mixed oxide systems, J. Phys. Chem. B 110 (2006) 23870–23880.
[18] Z.Z. Zhang, Y.Y. Liu, L.Y. Jia, C. Sun, B.J. Chen, R. Liu, Y.S. Tan, W.F. Tu, Effects of the reducing gas atmosphere on performance of FeCeNa catalyst for the hydrogenation of CO_2 to olefins, Chem. Eng. J. 428 (2022), 131388.
[19] J. Huang, S.Y. Jiang, M. Wang, X.X. Wang, J. Gao, C.S. Song, Dynamic evolution of Fe and carbon species over different ZrO_2 supports during CO prereduction and their effects on CO_2 hydrogenation to light olefins, ACS Sustain. Chem. Eng. 9 (2021) 7891–7903.
[20] J. Zhu, G.H. Zhang, W.H. Li, X.B. Zhang, F.S. Ding, C.S. Song, X.W. Guo, Deconvolution of the particle size effect on CO_2 hydrogenation over iron-based catalysts, ACS Catal. 10 (2020) 7424–7433.
[21] D. Fu, W. Dai, X. Xu, W. Mao, J. Su, Z. Zhang, B. Shi, J. Smith, P. Li, J. Xu, Y.-F. Han, Probing the structure evolution of iron-based fischer-tropsch to produce olefins by operando Raman spectroscopy, ChemCatChem 7 (2015) 752–756.
[22] Y.Y. Liu, B.J. Chen, R. Liu, W.Q. Liu, X.H. Gao, Y.S. Tan, Z.Z. Zhang, W.F. Tu, CO_2 hydrogenation to olefins on supported iron catalysts: effects of support properties on carbon-containing species and product distribution, Fuel 324 (2022), 124649.
[23] H.M.T. Galvis, J.H. Bitter, T. Davidian, M. Ruitenbeek, A.I. Dugulan, K.P. de Jong, Iron particle size effects for direct production of lower olefins from synthesis gas, J. Am. Chem. Soc. 134 (2012) 16207–16215.
[24] Z.H. Liu, X.H. Gao, B. Liu, W.L. Song, Q.X. Ma, T.S. Zhao, X. Wang, J.W. Bae, X. J. Zhang, J.L. Zhang, Highly stable and selective layered Co-Al-O catalysts for low-temperature CO_2 methanation, Appl. Catal. B- Environ. 310 (2022), 121303.
[25] J. Wei, R.W. Yao, Y. Han, Q.J. Ge, J. Sun, Towards the development of the emerging process of CO_2 heterogenous hydrogenation into high-value unsaturated heavy hydrocarbons, Chem. Soc. Rev. 50 (2021).
[26] E. de Smit, F. Cinquini, A.M. Beale, O.V. Safonova, W. van Beek, P. Sautet, B. M. Weckhuysen, Stability and reactivity of epsilon-chi-theta iron carbide catalyst phases in fischer-tropsch synthesis: controlling mu(c), J. Am. Chem. Soc. 132 (2010) 14928–14941.
[27] J. Zhu, P. Wang, X.B. Zhang, G.H. Zhang, R.T. Li, W.H. Li, T.P. Senftle, W. Liu, J. Y. Wang, A.F. Zhang, Q. Fu, C.S. Song, X.W. Guo, Dynamic structural evolution of iron catalysts involving competitive oxidation and carburization during CO_2 hydrogenation, Sci. Adv. 8 (2022) 5.
[28] Y.F. Xu, X.Y. Li, J.H. Gao, J. Wang, G.Y. Ma, X.D. Wen, Y. Yang, Y.W. Li, M.Y. Ding, A hydrophobic FeMn@Si catalyst increases olefins from syngas by suppressing C1 by-products, Science 371 (2021) 610–613.
[29] G. Kresse, J. Furthmuller, Efficiency of ab-initio total energy calculations for metals and semiconductors using a plane-wave basis set, Comp. Mater. Sci. 6 (1996) 15–50.
[30] G. Kresse, J. Furthmuller, Efficient iterative schemes for ab initio total-energy calculations using a plane-wave basis set, Phys. Rev. B 54 (1996) 11169–11186.
[31] P.E. Blochl, Projector augmented-wave method, Phys. Rev. B 50 (1994) 17953–17979.
[32] G. Kresse, D. Joubert, From ultrasoft pseudopotentials to the projector augmented-wave method, Phys. Rev. B 59 (1999) 1758–1775.
[33] J.P. Perdew, K. Burke, M. Ernzerhof, Generalized gradient approximation made simple (vol 77, pg 3865, 1996), Phys. Rev. Lett. 78 (1997), 1396-1396.
[34] J.P. Perdew, Y. Wang, Accurate and simple analytic representation of the electron-gas correlation-energy, Phys. Rev. B 45 (1992) 13244–13249.
[35] M. Methfessel, A.T. Paxton, High-precision sampling for brillouin-zone integration in metals, Phys. Rev. B 40 (1989) 3616–3621.
[36] H.J. Monkhorst, J.D. Pack, Special points for brillouin-zone integrations, Phys. Rev. B 13 (1976) 5188–5192.
[37] H. Jónsson, G. Mills, K.W. Jacobsen, Nudged elastic band method for findingminimum, in: B.J. Berne, G. Ciccotti, D.F. Coker (Eds.), Energy Paths of Transitions, Classical and Quantum Dynamics Condensed Phase Simulations WorldScientific, Hackensack, NJ, 1998, pp. 385–404.
[38] G. Henkelman, H. Jonsson, Improved tangent estimate in the nudged elastic band method for finding minimum energy paths and saddle points, J. Chem. Phys. 113 (2000) 9978–9985.
[39] S. Zhao, X.W. Liu, C.F. Huo, Y.W. Li, J.G. Wang, H.J. Jiao, Determining surface structure and stability of epsilon-Fe_2C, chi-Fe_5C_2, theta-Fe_3C and Fe_4C phases under carburization environment from combined DFT and atomistic thermodynamic studies, Catal. Struct. React. 1 (2015) 44–59.
[40] T.H. Pham, Y.Y. Qi, J. Yang, X.Z. Duan, G. Qian, X.G. Zhou, D. Chen, W.K. Yuan, Insights into flagg iron-carbide-catalyzed fischer-tropsch synthesis: suppression of CH_4 formation and enhancement of C-C coupling on chi-Fe_5C_2 (510), ACS Catal. 5 (2015) 2203–2208.
[41] H.T. Pham, X.Z. Duan, G. Qiang, X.G. Zhou, D. Chen, CO activation pathways of Fischer-Tropsch synthesis on χ-Fe_5C_2(510): direct versus hydrogen-assisted CO dissociation, J. Phys. Chem. C. 118 (2014) 10170–10176.
[42] X.F. Yu, J.L. Zhang, X. Wang, Q.X. Ma, X.H. Gao, H.Q. Xia, X.Y. Lai, S.B. Fan, T. S. Zhao, Fischer-Tropsch synthesis over methyl modified Fe_2O_3@SiO_2 catalysts with low CO_2 selectivity, Appl. Catal. B-Environ. 232 (2018) 420–428.
[43] M.H. Tan, S. Tian, T. Zhang, K.Z. Wang, L.W. Xiao, J.M. Liang, Q.X. Ma, G.H. Yang, N. Tsubaki, Y.S. Tan, Probing Hydrophobization of a Cu/ZnO Catalyst for Suppression of Water-Gas Shift Reaction in Syngas Conversion, ACS Catal. 11 (2021) 4633–4643.
[44] S. Zhao, X. Liu, C. Huo, Y. Li, J. Wang, H. Jiao, Surface morphology of Hägg iron carbide (χ-Fe_5C_2) from ab initio atomistic thermodynamics, J. Catal. 294 (2012) 47–53.
[45] J.T. Hu, L. Yu, J. Deng, Y. Wang, K. Cheng, C. Ma, Q.H. Zhang, W. Wen, S.S. Yu, Y. Pan, J.Z. Yang, H. Ma, F. Qi, Y.K. Wang, Y.P. Zheng, M.S. Chen, R. Huang, S. H. Zhang, Z.C. Zhao, J. Mao, X.Y. Meng, Q.Q. Ji, G.J. Hou, X.W. Han, X.H. Bao, Y. Wang, D.H. Deng, Sulfur vacancy-rich MoS_2 as a catalyst for the hydrogenation of CO_2 to methanol, Nat. Catal. 4 (2021) 242–250.
[46] Y.R. He, P. Zhao, J.Q. Yin, W.P. Guo, Y. Yang, Y.W. Li, C.F. Huo, X.D. Wen, CO direct versus H-assisted dissociation on hydrogen coadsorbed chi-Fe_5C_2 fischer-tropsch catalysts, J. Phys. Chem. C 122 (2018) 20907–20917.
[47] Y.R. He, P. Zhao, Y. Meng, W.P. Guo, Y. Yang, Y.W. Li, C.F. Huo, X.D. Wen, Hunting the correlation between Fe_5C_2 surfaces and their activities on CO: the descriptor of bond valence, J. Phys. Chem. C 122 (2018) 2806–2814.
[48] B.X. Chen, D. Wang, X.Z. Duan, W. Liu, Y.F. Li, G. Qian, W.K. Yuan, A. Holmen, X. G. Zhou, D. Chen, Charge-tuned CO activation over a chi-Fe_5C_2 fischer-tropsch catalyst, ACS Catal. 8 (2018) 2709–2714.
[49] J. Cheng, P. Hu, P. Ellis, S. French, G. Kelly, C.M. Lok, Chain growth mechanism in Fischer-Tropsch synthesis: a DFT study of C-C coupling over Ru, Fe, Rh, and Re surfaces, J. Phys. Chem. C 112 (2008) 6082–6086.
[50] J. Cheng, P. Hu, P. Ellis, S. French, G. Kelly, C.M. Lok, A DFT study of the chain growth probability in Fischer-Tropsch synthesis, J. Catal. 257 (2008) 221–228.
[51] Y.Y. Li, J. Hu, J. Xu, Y.P. Zheng, M.S. Chen, H.L. Wan, Q. Fu, F. Yang, X.H. Bao, Activation of CO and surface carbon species for conversion of syngas to light olefins on ZnCrOx-Al_2O_3 catalysts, Appl. Surf. Sci. 494 (2019) 353–360.
[52] W.F. Tu, C. Sun, Z.Z. Zhang, W.Q. Liu, H.S. Malhi, W. Ma, M.H. Zhu, Y.F. Han, Chemical and structural properties of Na decorated Fe_5C_2-ZnO catalysts during hydrogenation of CO_2 to linear α-olefins, Appl. Catal. B. -Environ. 298 (2021), 120657.
[53] X. Wang, Y.C. Hong, H. Shi, J. Szanyi, Kinetic modeling and transient DRIFTS-MS studies of CO_2 methanation over Ru/Al_2O_3 catalysts, J. Catal. 343 (2016) 185–195.
[54] A. Solis-Garcia, J.F. Louvier-Hernandez, A. Almendarez-Camarillo, J.C. Fierro-Gonzalez, Participation of surface bicarbonate, formate and methoxy species in the carbon dioxide methanation catalyzed by ZrO_2-supported Ni, Appl. Catal. B-Environ. 218 (2017) 611–620.
[55] A. Kaftan, M. Kusche, M. Laurin, P. Wasserscheid, J. Libuda, KOH-promoted Pt/Al_2O_3 catalysts for water gas shift and methanol steam reforming: an operando DRIFTS-MS study, Appl. Catal. B-Environ. 201 (2017) 169–181.
[56] S. Yang, H.-J. Chun, S. Lee, S.J. Han, K.-Y. Lee, Y.T. Kim, Comparative study of olefin production from CO and CO_2 using Na- and K-promoted zinc ferrite, ACS Catal. 10 (2020) 10742–10759.
[57] S.R. Docherty, C. Coperet, Deciphering metal-oxide and metal-metal interplay via surface organometallic chemistry: a case study with CO_2 hydrogenation to methanol, J. Am. Chem. Soc. 143 (2021) 6767–6780.